INTECH
open science | open minds

OPEN ACCESS
ARTICLE

Nanomaterials and Nanotechnology

Thermal Properties of TiO_2/PbS Nanoparticle Solar Cells

Regular Paper

Derek Padilla[1], Guangmei Zhai[2], Alison J. Breeze[3], Daoli Zhang[2], Glenn B. Alers[1] and Sue A. Carter[1,*]

1 Department of Physics, University of California, Santa Cruz, California, USA
2 Department of Electronic Science and Technology, Huazhong University of Science and Technology, Wuhan, People's Republic of China
3 Solexant Corporation, San Jose, California, USA
* Corresponding author E-mail: sacarter@ucsc.edu

Received 13 September 2012; Accepted 10 December 2012

Abstract Photovoltaic performance is shown to depend on ligand capping on PbS nanoparticle solar cells by varying the temperature between 140K and 350K. The thermal response of open-circuit voltage, short-circuit current density, fill-factor and shunt resistance varies between the ligands. A large increase in short-circuit current density at low temperatures is observed for 1,2-ethanedithiol and 3-mercaptopropionic acid and a relatively constant short-circuit current density is observed for the stiffer 1,4-benzenedithiol. Dark data provide evidence for tunnelling transport being the dominant charge conduction mechanism for all three ligand devices with recombination occurring within deep trap states. Under illumination, devices exhibit band-to-band recombination, indicated by an ideality factor of nearly unity.

Keywords Temperature, Charge Transport, Quantum Dot, Short-Circuit Current, Photovoltaic

1. Introduction

Thin-film quantum dot (QD) photovoltaics provide the potential to create high-efficiency devices while simultaneously achieving a low manufacturing cost due to reduced material costs and less expensive processing. The observation of multiple-exciton generation observed in PbS QD solutions at room temperature [1] motivates further research into such devices. Although much effort is focused on improving device performance through overall structure and QD properties, relatively few studies probe the effects of temperature or capping ligands on the photovoltaic (PV) parameters [2-5]. In solid-state applications, ligands are chosen to cap QDs based on their ability to effectively transfer energy within nanostructures as well as preventing the aggregation of nanoparticles. Thiols with short chains have demonstrated both properties, making them ideal candidates for use in PV devices [6]. Previous results show that cooling the PbS QD devices through the melting point of the ligand improves performance greatly through a six-fold increase in short-circuit current density (J_{sc}) at low temperatures [7]. This was attributed to the contraction of ligands, which increased the coupling between QDs, allowing for higher current densities. In addition to the ligands' thermal response within devices, the current-voltage-temperature parameter space reveals information regarding charge transport mechanisms.

Here, we present the effects of varying temperatures with three ligands used in PbS QD photovoltaic devices: 1,2-ethanedithiol (EDT), 3-mercapopropionic acid (MPA) and 1,4-benzenedithiol (BDT), by analysing current density-voltage (J-V) curves in dark and illuminated conditions. EDT, MPA and BDT were chosen based on their widely varying melting points (232 , 291K and 370K, respectively) and their comparatively higher open circuit voltage and short circuit currents compared to longer chain ligands We show that the increase in J_{sc} occurs upon cooling and varies with the choice of capping ligand. In addition, MPA devices exhibit dramatically different thermal responses, as seen in the fill factor (FF) and shunt resistance (R_{sh}) data.

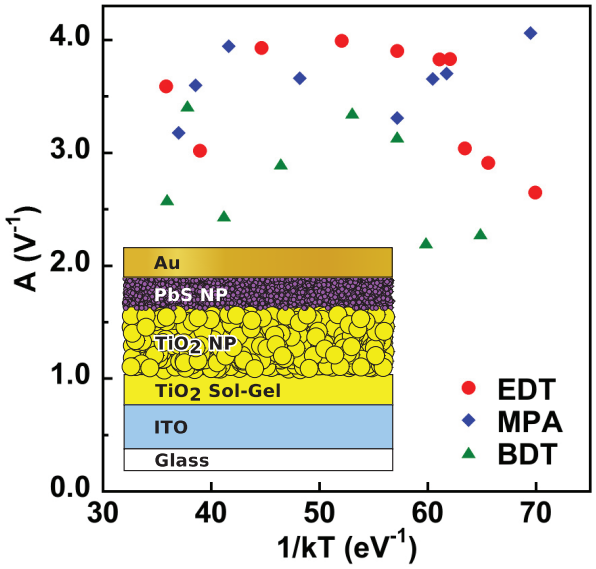

Figure 1. The exponential pre-factor of each ligand device obtained through fitting Eq. (1) to dark current-voltage data taken at different temperatures. Inset: Schematic of the TiO_2/PbS solar cell structure.

2. Experiments

The lead sulphide (PbS) quantum dots (QDs) were provided by Solexant and the titanium oxide (TiO_2) nanoparticles were purchased from Solaronix. The fabrication process follows the procedure published elsewhere [7] with the device structure shown in the inset of Figure 1. All devices use 3.9nm diameter PbS quantum dots, which correspond to an exciton peak of 1003nm and an optical energy gap of 1.24eV. Before the dipping process, the PbS QDs are submerged in a solution of chloroform and hexane with oleic acid as the capping ligand. The ligand exchange replaces oleic acid with the shorter ligands of EDT, MPA, or BDT for use in the devices (cf. Figure 2 inset). Current density-voltage (J-V) curves were taken from -1 to +1 V at varying temperatures in an Oxford cryostat with a Keithley 2400 source meter used a xenon light bulb next to the devices as the light source. The Xe bulb was chosen because it came closest to matching the solar spectrum in the region of interest (1000nm to 400nm) and exhibited no changes in intensity with temperature over the temperature region used in this study. The intensity was adjusted to match the J_{sc} of a commercial Si device under AM1.5, 100-mW/cm² illumination. After being fabricated in the nitrogen environment of the glove box, the devices were exposed to air for approximately five minutes while being transferred into the cryostat. Previous results show that this length of air exposure has a slightly positive effect on overall device performance [8]. While in the cryostat, nitrogen gas flowed across the devices. A RTD sensor placed next to the sample recorded the device temperature. Samples are warmed from the lowest temperature at a rate of ~15K/hr, followed by cooling at the same rate. For clarity, only cooling data is shown, with no appreciable hysteresis existing between cooling and warming data.

3. Results and Discussion

The transport mechanism of the devices was determined by fitting dark J-V data to the non-ideal diode equation

$$J(V,T) = J_0[\exp(A \times V) - 1], \quad (1)$$

where J_0 is the saturation current density and A is the exponential pre-factor. Both diode parameters in Eq. (1), J_0 and A can be temperature dependent, with the transport mechanism being determined by the way in which they vary with temperature [9]. Figure 1 demonstrates the weak temperature dependence of A as plotted against 1/kT. This, together with the negatively sloping linear behaviour of J_0 in the Arrhenius plot of Figure 2, is characteristic evidence of tunnelling transport [10].

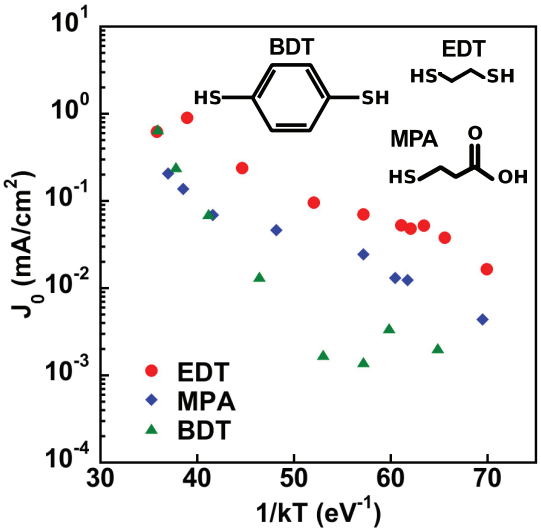

Figure 2. Arrhenius plot of the saturation current density for each ligand showing the negatively sloping linear behaviour. Inset: The chemical structures of the three capping ligands studied herein.

Figure 3 shows dark and light current density versus voltage (J-V) data for an EDT device at a range of temperatures from 166K to 324K. The dark current density at a positive bias of 1V shows two orders of magnitude increase from low to high temperatures, indicating that thermally excited charge carriers play an important role in conduction as T increases [11]. There is no appreciable distinction between dark J-V data from devices fabricated with the different ligands studied herein.

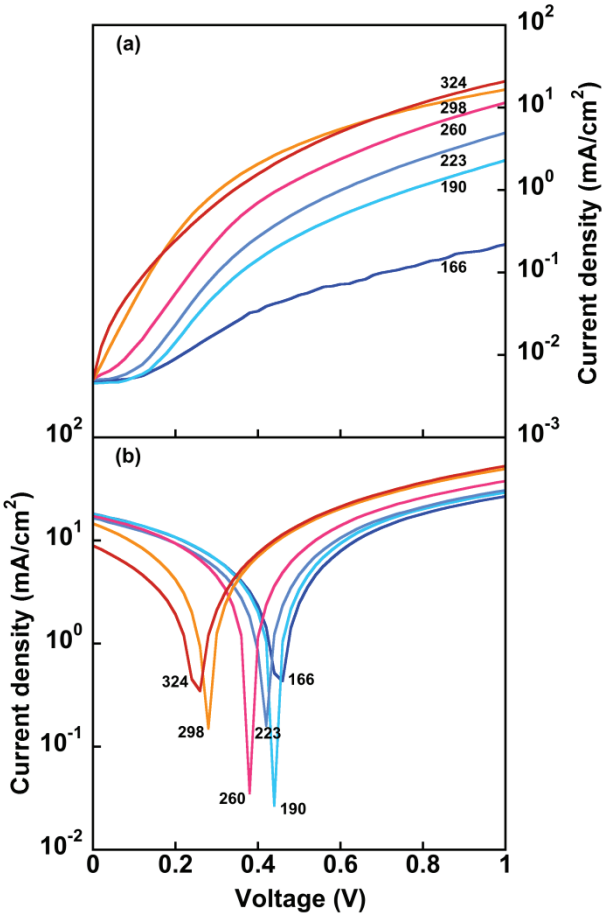

Figure 3. Current density-voltage data of an EDT device taken at 166, 190, 223, 260, 298 and 324K. (a) Dark J-V measurements. (b) J-V measurements under illumination. (Absolute temperatures are indicated on each J-V curve.)

Under illumination, the ligand-dependence of the devices is apparent in the PV parameters' temperature variations. Figure 4 shows the open-circuit voltage (V_{oc}) at a range of temperatures for devices using the three ligands. V_{oc} is expected to vary linearly with temperature [12]. However, a clear change in slope occurs when passing through room temperature for the EDT and MPA devices. BDT devices show the most linear V_{oc} temperature dependence. The small change that does occur is seen at higher temperatures than in the EDT and MPA devices.

Extrapolation of V_{oc}-T data to 0K provides the built-in potential (V_{bi}) of the devices [12], which indicates the difference in quasi-Fermi voltages between the TiO_2 and PbS layers. The V_{bi} for EDT, MPA and BDT devices are 0.59±0.02V, 0.56±0.03V and 0.57±0.02V respectively, indicating no significant ligand dependence of V_{bi}.

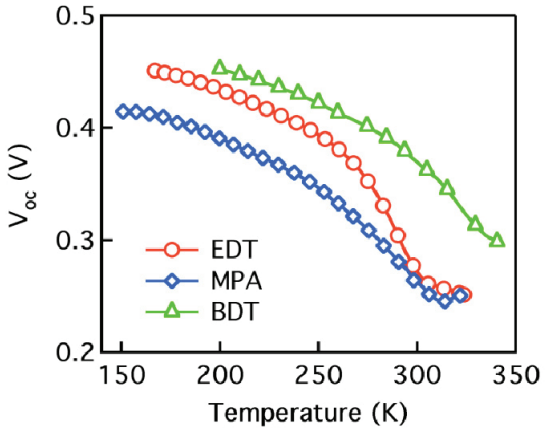

Figure 4. Open-circuit voltage dependence on temperature for three ligand devices. Extrapolating the flatter, low-temperature region yields built in potential values for EDT, MPA and BDT devices (see text).

The short-circuit current (J_{sc}) plotted as a function of temperature is shown in Figure 5. As with V_{oc}, both EDT and MPA exhibit a sharper change in J_{sc} than BDT. Both parameters' weaker dependence on temperature for BDT devices may be explained by BDT's more rigid structure. Comparing high-temperature to low-temperature J_{sc} values, the absolute change is similar for both EDT and MPA, however MPA shows an approximately eight-fold increase while EDT is closer to two-fold. BDT is relatively flat through the temperature range, though the shallow increase upon warming from below room temperature is consistent with previous results [13].

In FF-temperature data for the three ligand devices, both EDT and BDT are relatively temperature-independent (around 25%), while MPA sharply rises above room temperature from less than 20% to more than 35%. This is markedly different than the ligand-dependence shown in both J_{sc}- and V_{oc}-temperature data. The steep increase in FF occurs with a simultaneous rise in shunt resistance for MPA devices, as seen in Figure 6. Both of these together, however, do not lead to better device performance at high temperatures, mainly due to the low J_{sc} and V_{oc} values. This is demonstrated in Figure 7, showing J-V data for all three ligands at both 185K and 315K. The large R_{sh} for the MPA device at a high temperature is clearly the poorest performing J-V curve. It is also seen in Figure 7 that the device made with EDT demonstrates the best EQE at low temperatures as well as a significant thermal shift compared to MPA and, especially, BDT.

The discrepancy between dark and light current densities' response to cooling, as seen in the decrease in

positive-bias current density in Figure 3 and the increase in J_{sc} in Figure 5, can be reconciled by considering the weaker role of deep trap states under illumination. This can be verified by measuring an ideality factor of unity, indicating a direct, band-to-band recombination mechanism dominating transport, rather than recombination with charges in deep trap states. Attempting to obtain ideality factors for the devices using the dark current density from Eq. (1) yields non-unity values across the temperature range, leading us to believe that deep trap states play an important role in dark charge transport, which was previously seen to inhibit charge transport in PbS devices [14]. However, when examining devices under illumination, one may look at V_{oc} variations with light intensity, which should follow a linear trend on a semilogarithmic plot, with the slope being the ideality factor in units of thermal voltage [15]. We obtain a near unity ideality factor of 1.01 when using this technique, indicating that deep traps no longer play a significant role under illumination, which can be explained by the increased number of charge carriers filling the traps leaving mainly direct recombination processes when illuminated [15].

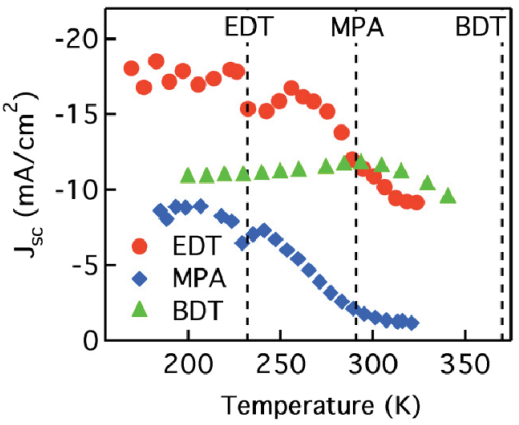

Figure 5. The variation of short-circuit current density with temperature for the three ligand devices. Vertical dashed lines show the melting point of each ligand.

J_{sc} dependence on temperature can partly be explained by the ligands freezing upon cooling. Previous studies have shown that ligand contraction in CdSe NP films lead to an order of magnitude decrease in transient times [16]. By varying the device ligand, we are able to verify that the freezing of the ligand does play a role in the PV properties of devices; however, not as clearly as this effect would suggest. With MPA's melting point being near room temperature (291K), much higher than EDT at 232K and BDT's being significantly higher than that at 370K, we should observe J_{sc} peaks at different temperatures based on which ligand is being used. This was not the case, as seen in Figure 5, although BDT does display significantly different behaviour. This difference may be attributed to the presence of a stiff benzene ring rather than the loose carbon chains found in EDT and MPA (cf. Figure 2 inset). The stability of the ring translates to much smaller changes in device performance upon cooling since the ligand is less susceptible to temperature variations.

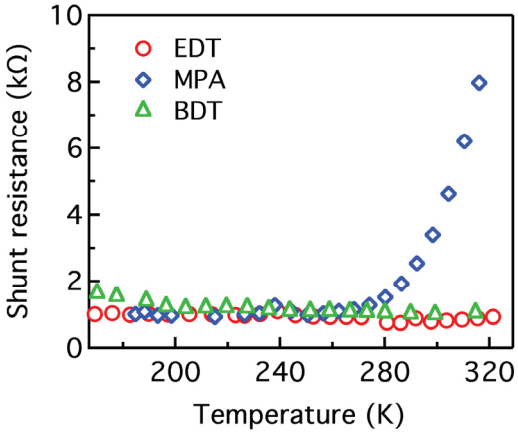

Figure 6. The shunt resistance dependence on temperature, showing MPA devices' large increase above room temperature.

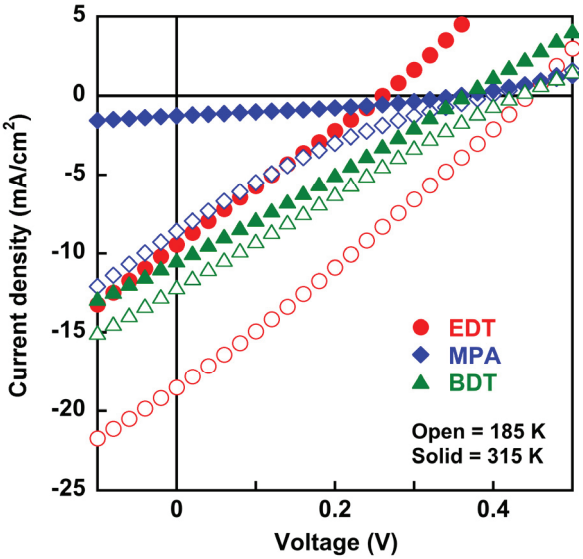

Figure 7. J-V characteristics for the photovoltaic devices fabricated with each of the three different ligands measured in the cryostat under illumination at both low temperature (185K) and high temperature (315K).

5. Conclusion

In summary, we have measured the effect of capping ligands in PbS NP ultrathin film photovoltaic devices at varying temperatures through current-voltage measurements. Short-circuit current density and open-circuit voltage show similar variations with temperature for EDT and MPA devices, both exhibiting an increase upon cooling below room temperature. J_{sc} and V_{oc} for BDT devices are relatively temperature independent, which we attribute to the stiffness of the benzene ring compared to linear carbon chains. MPA devices

demonstrate a sharp increase in fill-factor and shunt resistance upon warming through room temperature, however device performance is not improved due to the poor fill factor of MPA devices at warmer temperatures. The increase in dark current density upon warming is attributed to the significant role played by trap states, while light current density decreasing with higher temperatures is caused by the ligand contraction and saturation of trap states by the increased density of charge carriers when illuminated. These results indicate that even higher performance should be achievable through the careful selection of the coupling ligands.

6. Acknowledgments

D. Padilla acknowledges support from a Cota-Robles Fellowship and S. A. Carter acknowledges support from DOE Solar program award #1035478.

7. References

[1] Ellingson R J, Beard M C, Johnson J C, Yu P, Micic O I, Nozik A J, Shabaev A, Efros A L (2005) Highly Efficient Multiple Exciton Generation in Colloidal PbSe and PbS Quantum Dots. Nano Lett. 5: 865-871.

[2] Bakueva L, Musikhin S, Hines M A, Chang T-W F, Tzolov M, Scholes G D, Sargent E H (2003) Size-tunable infrared 1000–1600 nm electroluminescence from PbS quantum-dot nanocrystals in a semiconducting polymer. Appl. Phys. Lett. 82: 2895-2897.

[3] Jeong K S, Tang J, Liu H, Kim J, Schaefer A W, Kemp K, Levina L, Wang X, Hoogland S, Debnath R, Brzozowski L, Sargent E H, Asbury J B (2012) Enhanced Mobility-Lifetime Products in PbS Colloidal Quantum Dot Photovoltaics. ACS Nano 6: 89-99.

[4] Koleilat G I, Levina L, Shukla H, Myrskog S H, Hinds S, Pattantyus-Abraham A G, Sargent E H (2008) Efficient, Stable Infrared Photovoltaics Based on Solution-Cast Colloidal Quantum Dots. ACS Nano 2: 833-840.

[5] Luther J M, Gao J, Lloyd M T, Semonin O E, Beard M C, Nozik A J (2010) Stability Assessment on a 3% Bilayer PbS/ZnO Quantum Dot Heterojunction Solar Cell. Adv. Mater. 22: 3704-3707.

[6] Hammer N I, Emrick T, Barnes M D (2007) Quantum dots coordinated with conjugated organic ligands: new nanomaterials with novel photophysics. Nanoscale Res. Lett. 2: 282-290.

[7] Ju T, Graham R L, Zhai G, Rodriguez Y W, Breeze A J, Yang L, Alers G B, Carter S A (2010) High efficiency mesoporous titanium oxide PbS quantum dot solar cells at low temperature. Appl. Phys. Lett. 97: 043106.

[8] Zhai G, Bezryadina A, Breeze A J, Zhang D, Alers G B, Carter S A (2011) Air stability of TiO2/PbS colloidal nanoparticle solar cells and its impact on power efficiency. Appl. Phys. Lett. 99: 063512.

[9] Marsal L F, Pallares J, Correig X, Orpella A, Bardés D, Alcubilla A (1999) Analysis of conduction mechanisms in annealed n-SiC: H/p-crystalline Si heterojunction diodes for different doping concentrations. J. Appl. Phys. 85: 1216-1221.

[10] Park S, Cho E, Song D, Conibeer G, Green M A (2009) n-Type silicon quantum dots and p-type crystalline silicon heteroface solar cells. Sol. Energy Mater. Sol. Cells 93: 684-690.

[11] Kundu S, Roy S K, Banerji P (2011) GaAs metal-oxide-semiconductor device with titanium dioxide as dielectric layer: effect of oxide thickness on the device performance. J. Phys. D: Appl. Phys. 44: 155104.

[12] Hegedus S S, Shafarman W N (2004) Thin-film solar cells: device measurements and analysis. Prog. Photovolt: Res. Appl. 12: 155-176.

[13] Szendrei K, Speirs M, Gomulya W, Jarzab D, Manca M, Mikhnenko O V, Yarema M, Kooi B J, Heiss W, Loi M A (2012) Exploring the Origin of the Temperature-Dependent Behavior of PbS Nanocrystal Thin Films and Solar Cells. Adv. Funct. Mater. 22: 1598-1605.

[14] Barkhouse D A R, Pattantyus-Abraham A G, Levina L, Sargent E H (2008) Thiols Passivate Recombination Centers in Colloidal Quantum Dots Leading to Enhanced Photovoltaic Device Efficiency. ACS Nano 2: 2356-2362.

[15] Wetzelaer G A H, Kuik M, Lenes M, Blom P W M (2011) Determination of the trap-assisted recombination strength in polymer light emitting diodes. Appl. Phys. Lett. 99: 152506.

[16] Loef R, Houtepen A J, Talgorn E, Schoonman J, Goossens A (2009) Temperature Dependence of Electron Transport in CdSe Quantum Dot Films. J. Phys. Chem. C 113: 15992-15996.